Synthesis and in vivo evaluation of three fluid spray dried hybrid ciprofloxacin microparticles in Sprague Dawley rats

Article

Published Version

It is advisable to refer to the publisher's version if you intend to cite from the work. See Guidance on citing.

Synthesis and in vivo evaluation of three fluid spray dried hybrid ciprofloxacin microparticles in Sprague Dawley rats

Dina Dashty Mudher, Heshu Sulaiman Rahman, Sadat Abdulla Aziz, Amanpreet Kaur, Tareq Zeyad Bahjat & Hisham Al-Obaidi

Synthesis and in vivo evaluation of three fluid spray dried hybrid ciprofloxacin microparticles in Sprague Dawley rats

Dina Dashty Mudher[a], Heshu Sulaiman Rahman[b,c], Sadat Abdulla Aziz[d], Amanpreet Kaur[e], Tareq Zeyad Bahjat[e] and Hisham Al-Obaidi[e]

[a]Department of Biochemistry and Clinical Chemistry, College of Pharmacy, University of Sulaimani, Sulaimaniyah, Iraq; [b]Department of Physiology, College of Medicine, University of Sulaimani, Sulaimaniyah, Iraq; [c]Department of Medical Laboratory Sciences, Komar University of Science and Technology, Sulaimaniyah, Iraq; [d]Department of Basic Sciences, College of Veterinary Medicine, University of Sulaimani, Sulaimaniyah, Iraq; [e]Reading School of Pharmacy, University of Reading, Reading, UK

ABSTRACT

The aim of this study is to prepare and characterise mucoadhesive silica-coated silver nanoparticles loaded with ciprofloxacin (S-AgNPs-CSCFX), and investigate serum biochemical, haematological, and histo-pathological effects in Sprague Dawley rats upon oral administration. S-AgNPs-CSCFX microparticles were prepared using three fluid nozzle spray drying and characterised by scanning electron microscopy (SEM), X-ray dispersive spectrometry (EDX), transmission electron microscopy (TEM), Fourier transform infrared (FTIR), zeta potential and particles size measurements and X-ray powder diffraction (XRPD). Adult male Sprague Dawley rats were randomly divided between six-treated groups, including blank S-AgNPs and S-AgNPs-CSCFX (LD: Low dose; MD: Median Dose; HD: High Dose) and control group. Each group was treated daily to evaluate the effect of the prepared particles on the lipid profile, serum biochemical, hormonal level, haemogram, and vital organ histopathology. The results showed successful encapsulation of silver nanoparticles which resulted in spherical-shaped S-AgNPs-CSCFX with an average size of 1–5 μm and surface charge of 25.2 ± 5.52 mv. The in-vivo results showed that different doses of blank S-AgNPs and S-AgNPs-CSCFX had no significant toxic effects on the physiological, biochemical, and haematological parameters. There were no marked histopathological alterations in the vital organs of the treated rats with blank and loaded particles.

1. Introduction

Silver nanoparticles (AgNPs) have been the focus of extensive research due to their robust and broad antibacterial activity (Lee and Jun 2019). In addition, silver nanoparticles have been exploited in various biomedical applications, such as delivering anticancer agents, wound healing, dental applications, and implantable medical devices (Kumar et al. 2018). AgNPs have been well recognised for their broad-spectrum antimicrobial properties through targeting microbial DNA, peptides, and enzymes (Alavi and Rai 2019). Various hybrid nanoparticles using AgNPs as the core were prepared to synergise their antibacterial activity against Gram-negative and Gram-positive bacteria *in vitro* (Marin et al. 2015), including antibiotics such as ciprofloxacin (CFX) (Al-Obaidi et al. 2018; Liu et al. 2022), rifampicin (Farooq et al. 2019), vancomycin (Kaur et al. 2019), and minocycline (Chen et al. 2019).

The use of chitosan for forming microparticles has been widely attempted to help with mucuadhestion (Ways et al. 2018). Examples include incorporation of chitosan to help with deposition of inhaled drugs to aid with enhanced deposition and to prevent exhalation of smaller particles (Al-Obaidi et al. 2018). In another study, chitosan was used for its mucoadhesive properties to control the release and improve oral drug delivery of the

antiviral drug zidovudine (Pedreiro et al. 2022). A common method to form the microparticles is often based on ionic gelation in which chitosan is crosslinked using ionic crosslinking agent such as glutaraldehyde, formaldehyde, tripolyphosphate and polyaspartic acid sodium salt (Guadarrama-Escobar et al. 2023). This is based on exploiting the polycationic nature of the chitosan when dissolved at acidic conditions (Feng et al. 2015). This approach may reduce mucuadhesion as it will neutralize surface groups that are able to exert mucuadhesion.

Three fluid nozzle spray drying is relatively novel approach that has been used to spray dry drug and excipients that are not soluble in a mutual solvent (Al-Obaidi et al. 2018; Mohammed et al. 2020). Using this technology, we encapsulate silver coated silica nanoparticles inside a matrix of chitosan embedded with ciprofloxacin. The benefit of this approach is that it is removes the need for a linker and more importantly it will allow forming surface mucoadhesive coat of chitosan allowing burst release of the drug. To prevent aggregation of silver nanoparticles, the particles are coated with silica to form silica coated silver nanoparticles (S-AgNPs). This enhances stability of the formed particles and offers greater control for the dissolution of entrapped silver and drug (Al-Obaidi et al. 2018).

In this work, we use three fluid nozzle spray drying to form core/shell microparticles in which the shell is made up of low molecular weight chitosan (CS) with the antibiotic drug ciprofloxacin while the core is made up of silica coated silver nanoparticles. The surface of the formed microparticles allows mucuadhesion thanks to the presence of the cationic chitosan while the core allows burst deposition of the silica coated silver nanobeads. We use this approach to maintain chitosan in its natural form rather than forming cross linked network using a linker. The use of three fluid nozzle spray drying adds another level of control in particle engineering to ensure formed particles exhibit the desired core/-shell structure. In addition, to the authors knowledge, there is no evaluation of the *in vivo* safety of S-AgNPs-CSCFX; thus, in this study, we aim to synthesize, characterise, and determine the toxicological effects of S-AgNPs-CSCFX microparticles that were administered *via* the oral route in healthy rats. Analysis of prepared particles included a range of haematological, biochemical and histopathological assessments.

2. Materials and methods

2.1. Materials

Tetraethyl orthosilicate (TEOS; ≥99.0%), silver (Ag; nanopowder, <100 nm particle size, 99.5% trace metals basis), low molecular weight chitosan (CS), dimethylamine solution (DMA; 40% in water), and acetic acid (ReagentPlus®, ≥99%) were obtained from Sigma Aldrich, USA, while ciprofloxacin (CFX; ≥98.0%) and anhydrous lactose were ordered from Fluka, USA, and Ethanol absolute (VWR International, Leicestershire, UK).

2.2. Preparation of silica only and silica-coated Ag nanoparticles

Two fluid nozzle spray drying (Buchi B290 mini spray dryer, Switzerland) was used to prepare the silica only nanoparticles using nozzle size of 0.7 mm. The method of forming the silica particles or silica coated silver nanoparticles was based on Stöber method and as described in the literature (Kobayashi et al. 2005; Jarvie et al. 2009). Briefly, 75 ml EtOH and 20 ml distilled water was mixed, then 1.0 ml DMA was added and ultra-sonicated. This was followed by the addition of 0.5 ml TEOS to the previous solution and vigorously stirred. To prepare the AgNPs, the same procedure was followed with slight modification: Ag was suspended in the EtOH/water solution followed by TEOS addition which was then ultrasonicated to prevent aggregation. As a result, the amount of added Ag to the spray drying solution was equivalent to 0.17% (w/v) and was guided by the approximate final content of spray-dried particles (≈ 2%, w/w).

2.3. Preparation of silica-coated AgNPs loaded CS/CFX by three fluid spray drying

Three-fluid nozzle spray drying (Buchi B290 mini spray dryer, Switzerland) was used to prepare the hybrid AgNPs-CSCFX. Briefly, CFX (3.5 g) and CS (0.5 g) were added to 3% (v/v) acetic acid and vigorously stirred for complete dissolution. Then, the produced S-AgNPs suspension was injected in the internal nozzle, while the CS/CFX with the acetic acid solution was pumped through the external feed nozzle. The spray-dried suspensions resulted in solid particles with an Ag content of 2% (w/w). Content analysis was performed to determine CFX content in the final spray dried particles. This was carried out *via* dissolving 20 mg of powder in 100 ml of 3% (v/v) acetic acid followed by appropriate dilution prior to measurement of absorption at wavelength 277 nm using UV spectrophotometer (Jenway, Staffordshire, UK). The yield following spray drying varied between 30–50% per sample.

2.4. Characterisation of spray-dried powders by scanning electron microscopy (SEM)

SEM (Scanning Electron Microscopy) (Microscope: FEI Quanta 600 FEG SEM) was used to examine the shape, surface, morphology, and microstructure of the particles. The prepared microparticle samples were mounted on aluminum stubs (Pin stub 12.5 mm aluminum with groove 8 mm pin) with double-sided adhesive carbon tabs (Leit Adhesive Carbon Tabs 12 mm). All samples were coated twice with carbon fiber. Edwards Sputter Coater (S150B) was used to gold coat the samples for images taken under high vacuum. All specimens were then imaged at an accelerating voltage of 20 kV at different magnifications ranging from 100X to 10000X.

2.5. Transmission electron microscopy (TEM)

TEM was run on selected samples to define their shape and size using a Philips Tecnai T20 microscope at 200 kV provided with a dispersive energy spectrum (EDS) detector. A drop of sample (silica coated nanoparticles inside matrix of CFX and CFX/chitosan) suspended in 0.1 ml deionized water was placed on a carbon-film coated copper grid at 200 kV of a transmission electron microscope (TEM Philips Tecnai T20, Philips Ltd, Tokyo, Japan). After drying for 20 min, the copper grid was fixed onto the sample holder and placed in a vacuum chamber. TEM images were captured under low vacuum using print magnifications of 260000x and 51900x.

2.6. Energy dispersive X-ray (EDX) analysis

X-ray dispersive spectrometry was used to understand the chemical composition at the surface of the prepared particles. Three different sites of interest for each sample were examined using EDX analysis using a scanning electron microscope (SEM) (operated at 20 kV) with an X-ray detector using same method described above for SEM samples. This method identifies the atomic composition and characterises the spatial chemical distribution of the sample.

2.7. X-ray powder diffraction (XRPD)

Bruker D8 Advance X-ray diffractometer (Bruker AXS GmbH, Germany), a Cu-source, theta–theta diffractometer with a Lynx eye position sensitive detector (40 kV voltage and 40 mA current) was used. DFFRAC plus XRD commander software (Bruker AXS GmbH, Germany) with a 2θ range of 5–45°, a step size of 0.02° and a time per step of 1.33 s was used to analyze the scanned samples.

2.8. Characterisation of spray-dried powders by Fourier Transform infrared spectroscopy (FTIR)

Fourier transform infrared (FTIR) spectra measurements were collected for all spray-dried samples using a Perkin-Elmer Spectrum 100 FTIR spectrophotometer, over a scan range of 650–4200 cm^{-1} with an average of 16 scans. The effect of carbon dioxide was eliminated by obtaining a background spectrum for each experimental condition.

2.9. Dynamic light scattering (DLS) and zeta potential measurements

Samples were diluted to 1 ml with ultra-pure water and transferred to a glass cuvette and analyzed using a Zetasizer (Malvern Zetasizer nano series, UK). The refractive index and viscosity of distilled water were used as reference values. A series of dilutions were made to ensure consistent scattering and to avoid multiple scattering. The temperature was set at 25 °C and each sample was allowed to equilibrate for 60 s and a total of 12 runs per measurement were performed with 10 s per run. Z-average diameter in nm obtained represented the particle size of the samples. Zeta potential analysis was undertaken using electrophoretic light scattering (Malvern Zetasizer nano series, UK). Every sample was diluted to the same extent as in size analysis using deionized water before measurement. All results were recorded as the mean of three repeats.

2.10. In vivo study: preparation of animals

Male 6–8 weeks Sprague Dawley rats (100–125 g) were received by the Department of Biology, College of Science, University of Tikrit, Iraq. The rats were acclimatized for 7 days with a 12-h dark/-light cycle at 25 ± 2 °C.

2.11. Subchronic toxicity protocol

Animals ($N = 28$) were randomly allocated to 7 groups ($N = 4$): (i) normal control drenched with distilled water (CN: Control Negative); oral treatment with (ii) AgNPs-CSCFX (LD: Low dose, 30 mg/Kg body weight); (iii) AgNPs-CSCFX (MD: Median Dose, 60 mg/Kg body weight); (iv) AgNPs-CSCFX (HD: High Dose, 90 mg/Kg body weight), (v) Blank AgNPs without CFX (LD: Low Dose, 30 mg/Kg body weight), (vi) Blank S-AgNPs without CFX (MD: Median Dose, 60 mg/Kg body weight), and (vii) Blank S-AgNPs without CFX (HD: High Dose, 90 mg/Kg body weight). The powders of blank and loaded NPs were prepared in 1% glacial acetic acid. All drenching processes were done using a force-feeding, ball-tipped needle; for exactly 3 consecutive weeks. The body weights were measured on days 0, 7, 14, and 21 using a scientific measuring scale. Every morning, the animals were investigated for behavioral abnormality, unusual symptoms, food intake, and gross appearance.

2.12. Collection of biochemical parameters

On days 22 and 24 h after cessation of the last treatments, animals were deeply anesthetized using xylazine/ketamine solution. Blood samples (10 ml/rat) were obtained via cardiac puncture, and serum was collected (from half of the blood) by centrifugation (3500 rpm for 10 min). The level of serum total protein (TP), albumin (ALB), globulin (GLB), total serum bilirubin (TSB), alanine aminotransferase (ALT), aspartate aminotransferase (AST), alkaline phosphatase (ALP) (liver function tests), urea, and creatinine, total calcium, phosphate, (Kidney function tests) were determined using standard diagnostic kits. Additionally, serum levels of lipid profile include total cholesterol (TC), low-density lipoprotein (LDL), high-density lipoprotein (HDL), very low high-density lipoprotein (VLDL), and triglyceride (TG) were determined using a biochemical analyzer (Accent 200, Cormy, Poland) with prolactin (PCT) values using Cobas e601 (Roche, Germany).

2.13. Hematological assessment

A blood samples (5 ml) was transferred to ethylene-diamine tetra-acetic acid (EDTA) tubes, mixed well, and analyzed immediately. The complete blood count (CBC), including total red blood cells (RBC), hemoglobin (Hgb), hematocrit (HCT), Mean Corpuscular Volume (MCV), Mean Corpuscular Hemoglobin (MCH), Mean Corpuscular Hemoglobin Concentration (MCHC), RDWC, RDWS, together with total and differential white blood cells (WBC), platelets (PLT), Mean Platelet Volume (MPV), Platelet Distribution Width (PDW), and Platelet-Large Cell Ratio (PLCR) in each sample were measured by an automatic hematology analyzer (Mythic 22, Orphee, Switzerland).

2.14. Histopathological examination

Immediately after animal sacrifice (at necropsy), samples of the liver and kidneys were collected, rinsed in normal saline, and examined for grossly visible lesions. About 1.0 g from each tissue was processed (fixed in 10% formalin for two nights, dehydrated, paraffin-embedded, rehydrated, and sliced into 3.0 μm thick) for histopathological examination using previously established methods.(Crissman et al. 2004) The sections were then stained with Harris's hematoxylin and eosin (H&E), then fixed with DPX, observed under the light microscope, and photos were captured.

2.15. Data analysis

The data were analyzed using SPSS version 25.0 (Chicago, USA) and data were expressed as mean ± SD. One-way analysis of variance (ANOVA) and Post hoc comparison tests was done using the Tukey's-b, Bonferroni and Duncan test. Probability values of <0.05 were considered statistically significant.

3. Results

3.1. Physicochemical characterisation of prepared spray dried microparticles

Silica agglomerates of small nanoparticles of approximately 100 nm were produced by 2-fluid spray drying with a size of agglomerates varied between 1 to 4 μm (Figure 1(A)). The particles maintained this structure when Ag was incorporated exhibiting similar size range (Figure 1(B)). When CFX was added in, the surface of the particles became less smooth indicating possible deposition of the drug at the surface (Figure 1(C)). Particles that included chitosan (i.e. S-AgNPs-CSCFX) were irregular in shape with surface showing entangled chitosan chains across the silica coated silver agglomerates (Figures 1(D)). Size analysis of the entrapped silica coated silver nanoparticles showed a size of 87 nm which agreed well with the SEM images.

Further analysis of the surface using EDX analysis showed a consistent trend in which the surface of the silica only nanoparticles had the highest Si content (expressed as %weight) (Figure 2(A)). The amount of Si decreased slightly in S-AgNPs which may indicate the presence of free Ag deposited on the surface. The ratio decreased considerably in S-AgNPs-CFX and S-AgNPs-CSCFX to approximately 10% (weight %) suggesting that the surface has been covered by the CFX/CS. Theoretically, a complete coverage should result in no Si at the surface hence results suggest partial but successful coating of the particles which agreed with the SEM images in Figure 1. When comparing the content of Ag, the data agreed with analysis above as it shows high abundance in S-AgNPs which indicates presence of silver on the surface (Figure 2(B)). Amount of silver is significantly lower in S-AgNPs-CFX and S-AgNPs-CSCFX signifying the successful entrapment of silver within the silica/CFX/CS matrix. Zeta potential measurements revealed the following results: silica only particles -33.2 ± 10.7 mv,
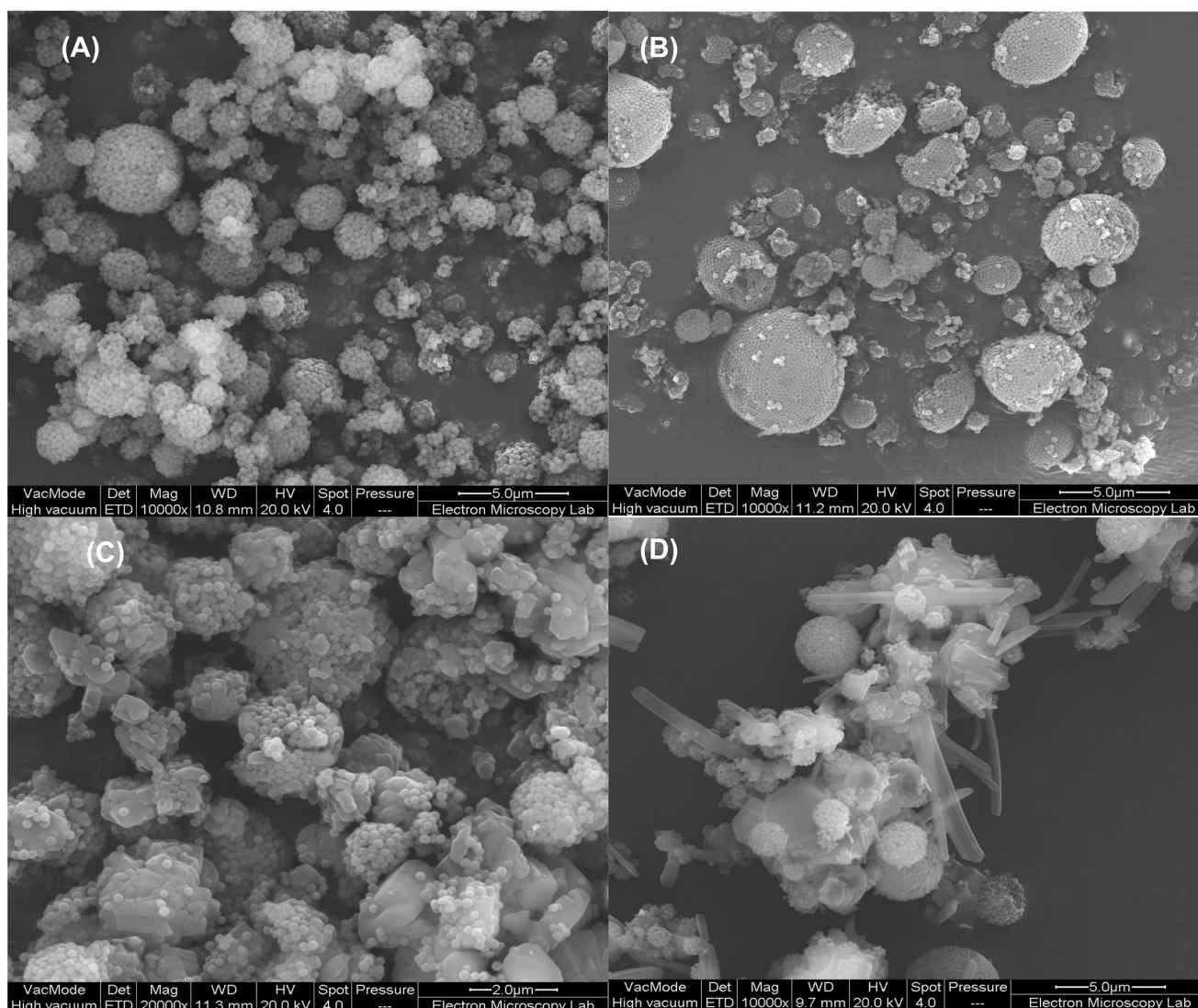
Figure 1. Scanning electron microscopy (SEM) images of silica nanoparticles prepared by 2-fluid nozzle spray drying (A), silica coated silver nanoparticles prepared by 2-fluid nozzle spray drying (B), silica coated silver nanoparticles and entrapped with a layer of CFX prepared by 3-fluid nozzle spray drying (C) and silica coated silver nanoparticles inside CFX/chitosan prepared by 3-fluid nozzle spray drying (D).

silica coated silver nanoparticles − 38.7 ± 6.19 mv, silica coated silver with CFX − 40.4 ± 8.19 mv and silica coated silver nanoparticles with CFX and chitosan 25.2 ± 5.52 mv.

To confirm the above findings, the samples were further analysed to assess molecular interactions and surface morphology. As can be seen in Figure 3, the results showed broadening in carbonyl group stretching of CFX at 1612 cm^{-1}. The ionised COO-can be seen as symmetric and asymmetric vibrations at 1585 and 1375 cm^{-1} respectively (Mohammed et al. 2020). Among assigned peaks, it is clear that there is a significant shift in peaks positions 1612, 1585, 1540, 1499, 1282 cm^{-1}. CFX is known to exhibit a zwitterion behavior due to electronic cloud movement promoting ionization (Mohammed et al. 2020). This pattern, however, is altered when hydrogen bonds are formed minimising deprotonation. This suggests molecular interactions with the chitosan chain, which is rich with hydrogen bond donor groups.

X-ray powder diffraction (XRPD) data showed that the silica particles were completely amorphous, while the entrapment of Ag can be clearly seen with the lower intensity of peak at 2θ of 38° which is typically found in pure crystalline Ag (Figure 4). When CFX was included, some signs of crystalline residues could be seen, while embedding with chitosan almost led to completely

amorphous dispersions (Figure 2). Residual peak of 2θ of 38° could still be seen in S-AgNPs-CFX and S-AgNPs-CSCFX which further supports above SEM and EDX results. Overall, these results confirm that the produced particles were predominantly amorphous with evidence for total or partial encapsulation of Ag inside the CFX/CS matrix.

Dissolution was evaluated using transmission electron microscopy (TEM) using same approach used before (Al-Obaidi et al. 2018) (Figure 5). As can be seen, particles dissolution was seen to release the entrapped particles as aggregates of multiple silica coated Ag particles which were seen as dark dots. The particles can be seen to completely dissolve showing traces of the dissolved silica. These results confirmed the successful design of the particles which could dissolve to release the entrapped silver nanoparticles.

3.2. In vivo *assessment of clinical vital signs*

In vivo assessment of clinical vital signs revealed no signs of toxicity such as behavioral change, segregation, laying down, mortality, ruffled hair, cannibalism, or loss of appetite. Weight change is considered a vital toxicity index for tested laboratory animals; as
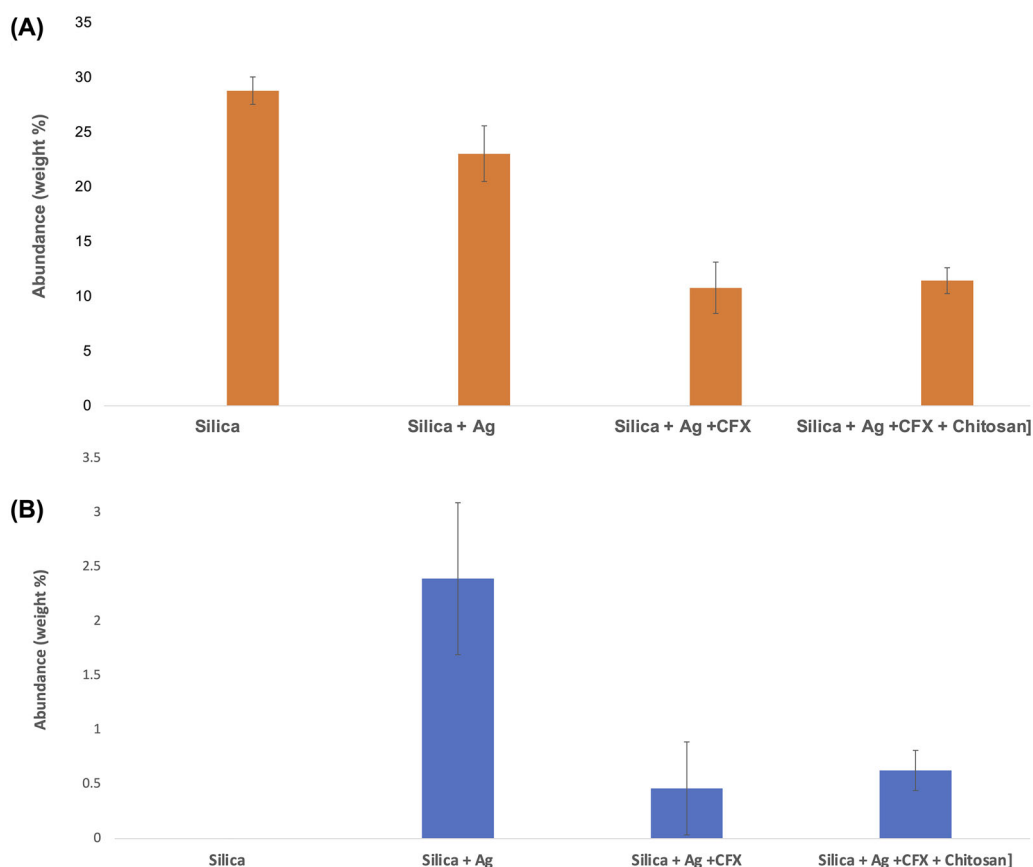
Figure 2. X-ray dispersive spectrometry (EDX) results showing surface abundance of (A) silicon (Si) and (B) silver (Ag) of samples prepared by spray drying.
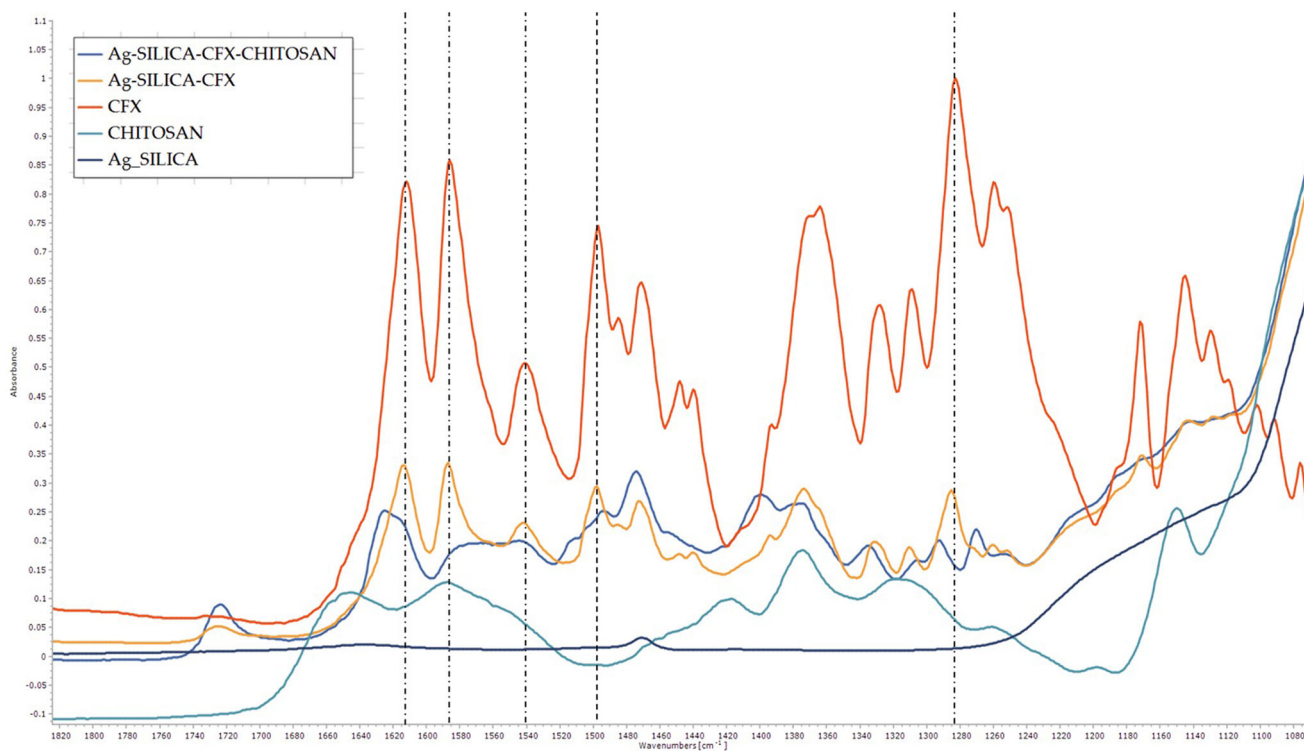
Figure 3. FTIR spectra of prepared solid dispersions prepared using two and 3-fluid nozzle spray drying along with corresponding spectra for ciprofloxacin (CFX) and chitosan. The dotted lines show peak positions in CFX where a shift was seen compared to S-AgNPs-CSCFX microparticles signifying structural changes.
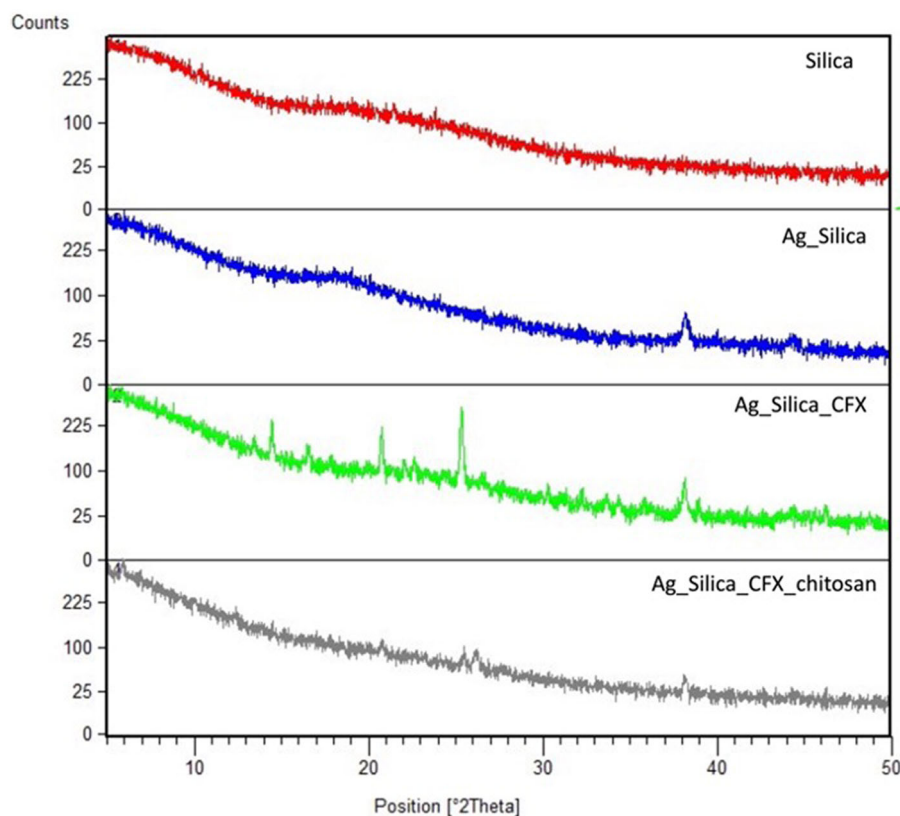
Figure 4. X-ray powder diffraction diffractograms of spray dried microparticles of silica, silica coated silver particles, silica coated silver nanoparticles loaded with CFX, and silica coated silver nanoparticles loaded with CFX and chitosan.
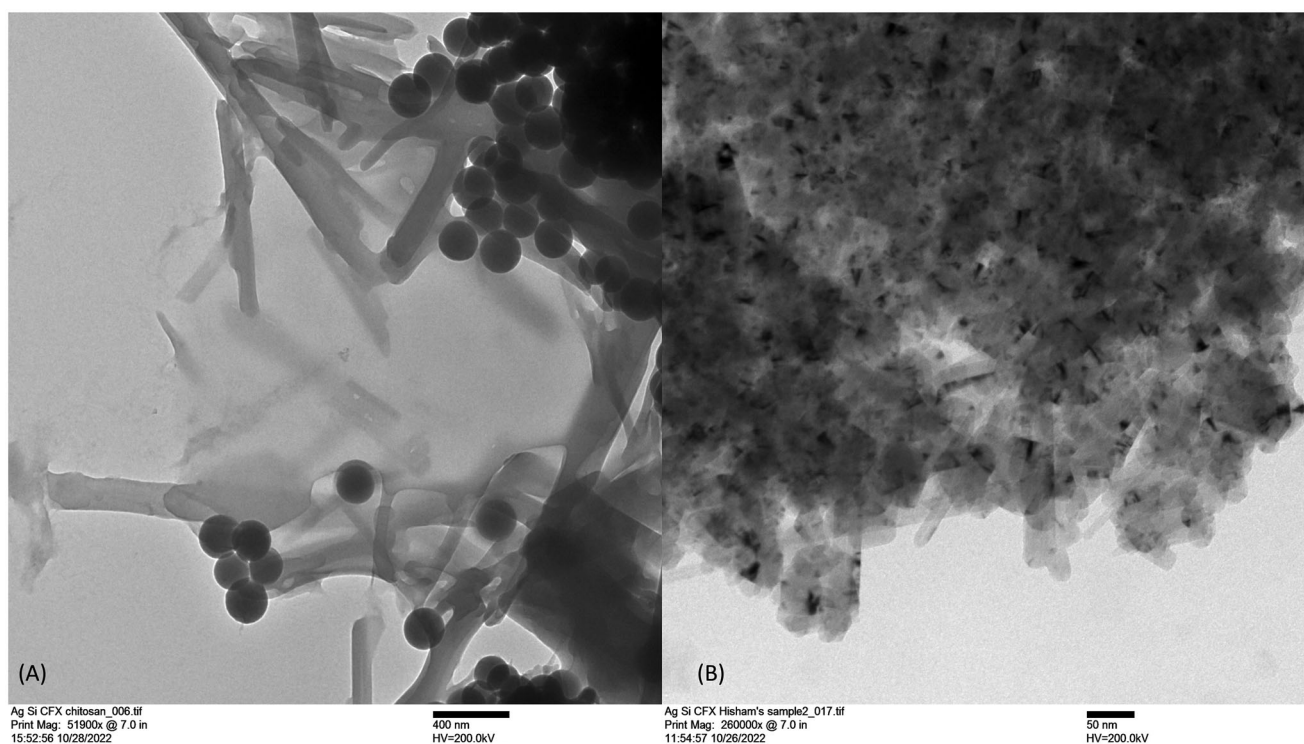
Figure 5. Transmission electron microscopy (TEM) images showing dissolution of silica coated nanoparticles inside matrix of CFX/chitosan (A) and CFX (B) prepared by 3-fluid nozzle spray drying.

significant body weight reduction is a dangerous sign of toxic products in treated animals. This study measured the animal's body weight before dosing (day 0) and after 7, 14, and 21 days of starting treatment. Control group and treated animals with various doses of blank and loaded NPs showed significant steady increment in body weight ($p < 0.05$), while there were not any

Table 1. Body weight of rats treated with blank and loaded silica-coated silver nanoparticles with ciprofloxacin.

Time Treatments	Day-0	Day-7	Day-14	Day-21
Control Negative	^{A} 136.2 ± 1.83^A	^{A}162.7 ± 28.80^A	^{A}188.50 ± 40.27^A	^{A}205.7 ± 54.71^A
blank LD	^{A}125.5 ± 9.13^{AB}	^{AB}143.2 ± 10.99^A	^{B}167.2 ± 15.77^A	^{BC}183.7 ± 10.40^A
blank MD	^{A}138.2 ± 7.72^{AB}	^{B}174.5 ± 11.73^A	^{BC}196.2 ± 9.98^A	^{C}210.0 ± 12.66^A
blank HD	^{A}138.0 ± 8.32^{AB}	^{AB}157.2 ± 16.74^A	^{B}179.2 ± 27.97^A	^{BC}197.5 ± 11.96^A
Loaded LD	^{A}140.7 ± 4.39^{AB}	^{B}168.2 ± 16.78^A	^{BC}189.7 ± 10.71^A	^{C}209.2 ± 14.08^A
loaded MD	^{A}150.2 ± 10.61^B	^{B}174.7 ± 13.63^A	^{BC}198.7 ± 12.92^A	^{C}216.7 ± 9.25^A
loaded HD	^{A}139.5 ± 9.13^{AB}	^{AB}167.3 ± 10.96^A	^{BC}186.2 ± 8.54^A	^{C}197.5 ± 7.02^A

*CN: Control negative; LD: Low dose (30 mg/Kg body weight); MD: Median Dose (60 mg/Kg body weight); and HD: High Dose (90 mg/Kg body weight); S-AgNPs: Silica coated silver nanoparticles; S-AgNPs-CSCFX: Silica coated silver nanoparticles loaded with ciprofloxacin.

The data are mean ± Std. Deviation. Bonferroni Post Hoc test was used. The superscript letters on the right of each data represent the statistical differences between groups. While the superscripts letters on the left represent the statistical differences within the groups. P-value less than 0.05 was considered statistical differences.

Table 2. Serum liver function tests of rats treated with blank and loaded silica-coated silver nanoparticles with ciprofloxacin.

Test Group	Total protein (TP) (g/L)	Albumin (ALB) (g/L)	Globulin (GLB) (g/L)	Alanine Aminotransferase (ALT) (U/L)	Aspartate Aminotransferase (AST) (U/L)	Alkaline Phosphatase (ALP) (U/L)	Total Serum Bilirubin (TSB) (?mol/L)
CN	6.03 ± 0.24^a	3.4 ± 0.07^a	3.55 ± 75.15^a	85.25 ± 28.77^a	142.5 ± 12.84^a	595.25 ± 86.04^b	0.0 ± 0.0^a
LD-S-AgNPs	6.07 ± 0.15^a	3.4 ± 0.1^a	3.93 ± 1.25^a	82.0 ± 3.51^a	169.0 ± 15.72^a	563.67 ± 67.77^b	0.0 ± 0.0^a
MD-S-AgNPs	7.03 ± 0.11^c	3.7 ± 0.11^{ab}	3.2 ± 0.11^a	73.75 ± 5.66^a	159.25 ± 24.77^a	480.75 ± 41.58^{ab}	0.0 ± 0.0^a
HD-S-AgNPs	6.43 ± 0.17^{ab}	3.63 ± 0.14^{ab}	2.8 ± 0.11^a	89.5 ± 23.6^a	192.0 ± 23.23^a	500.75 ± 84.17^b	0.0 ± 0.0^a
LD-S-AgNPs-CSCFX	7.08 ± 0.11^c	4.08 ± 0.08^c	3.0 ± 0.08^a	95.25 ± 6.49^a	172.25 ± 12.17^a	507.5 ± 36.36^b	0.023 ± 0.023^a
MD-S-AgNPs-CSCFX	6.75 ± 0.12^{bc}	3.8 ± 0.0^{bc}	2.95 ± 0.12^a	88.50 ± 7.9^a	161.25 ± 5.34^a	549.75 ± 55.65^b	0.0 ± 0.0^a
HD-S-AgNPs-CSCFX	6.83 ± 0.26^{bc}	3.95 ± 0.16^{bc}	3.08 ± 0.27^a	63.0 ± 6.15^a	144.25 ± 15.61^a	406.5 ± 26.08^a	0.0 ± 0.0^a

CN: Control negative; LD: Low dose (30 mg/Kg body weight); MD: Median Dose (60 mg/Kg body weight); and HD: High Dose (90 mg/Kg body weight); S-AgNPs: Silica coated silver nanoparticles; S-AgNPs-CFX: Silica coated silver nanoparticles loaded with ciprofloxacin.
Superscripts on the right of the means indicate statistical differences ($p < 0.05$) between the groups. Values are means ± standard error. Values are means ± standard errors for $N = 4$. Statistical analysis was by one way ANOVA.

significant differences between the weight of the groups when compared to each other at the same time point throughout the course of the treatment (days 7, 14, and 21) (Table 1).

Regarding the serum biochemical tests, there was no significant elevation of liver function tests (except for AST) ($p > 0.05$) (Table 2) and renal function tests (Table 3) in treated animals with blank and loaded AgNPs related to the control group. Subsequently, treated rats with blank and loaded AgNPs resulted in significant increment ($p < 0.05$) in TG and VLDL with no substantial changes in other lipid profile tests and prolactin values (Table 4). Regarding the hematological tests, no significant differences were seen in all tests in treated animals with various doses of blank and loaded AgNPs except for WBC, lymphocyte, monocyte, and granulocyte values, where the changes were significant in treated animals compared to control group ($p < 0.05$) (Table 5). Furthermore, histopathological observation showed no toxicological lesions with no remarked differences in the renal and hepatic histological structures in the control and the treated groups with various doses of blank and loaded AgNPs for three consecutive weeks.

3.3. Histopathological findings

Liver sections of treated animals did not show signs of destructed hepatic cell cords, polyploidization, presence of inflammatory cells, focal lymphocytic infiltration, dilation of sinusoidal space, eosinophilic cytoplasm, and pyknotic nuclei of hepatocytes. Also, there were no membrane leakage, necrosis, and/or apoptosis. Similarly, the overall structure of the liver, hepatocytes, sinusoids, portal triads, and central veins were normal. However, some groups of treated animals saw mild Kupffer cell proliferation with mild hydropic degeneration (Figure 6). Meanwhile, the kidney sections of treated rats exhibited normal structure and appearance of glomeruli/tubules. The proximal convoluted tubules (PCT), distal convoluted tubules (DCT), and macula densa were intact with no

Bowman's capsule thickening and interstitial inflammation. As can be seen in Figure 6, liver section showed no significant morphological changes, evident by normally radiated column of hepatocytes (HP) surrounding mildly widened central vein (CV) with distinctively dilated sinusoidal capillaries. On the other hand, Low dose group (G2) treated with 30 mg/kg of S-AgNPs-CSCFX, reveal mild to moderate vacuolar degeneration (VD) with clear hydropic changes. The section reveals dilated central vein (CV) together with normally appeared sinusoidal capillaries (S).

Medium dose group treated with 60 mg/kg of S-AgNPs-CSCFX, demonstrated the presence of moderate to significant hydropic degeneration (HD). On the other hand, it showed some typically appeared hepatocytes around the central vein (CV). High dose group treated with 90 mg/kg of S-AgNPs-CSCFX, showed more significant vacuolar degenerations (VD). This revealed area of some normally distributed hepatocytes (HP) together with typical sinusoidal capillaries, disseminated structurally around the central vein (CV). Low dose group treated with 30 mg/kg of blank S-AgNPs, showed moderate vacuolar degenerations (VD), together some areas of dilated and congested sinusoidal capillaries (yellow arrows). Presence of ordinary arranged hepatocytes (HD) around the central vein (CV) with no obvious congestion. Medium dose group treated with 60 mg/kg of blank S-AgNPs, show significant vacuolar degenerations (VD) within the hepatocytes, together with regular sinusoidal capillaries, and perfectly arranged hepatocytes column around the central vein (CV) with evident vascular congestion. High dose group treated with 90 mg/kg of blank S-AgNPs. Presence of eosinophilic proteinaceous fluid within the central vein lumen (CV), together with slightly severe vacuolar and hydropic degenerations (VD, HD). In addition to, the section reveals some centrilobular area of typically appeared parenchymal cell around the central vein (CV).

In vivo results were compared to the findings in kidneys as shown in Figure 7. Some groups of treated animals detected low-

Table 3. Serum kidney function tests of rats treated with blank and loaded silica-coated silver nanoparticles with ciprofloxacin.

Test Group	Urea (mmol/L)	Creatinine (µmol/L)	Total Calcium (mmol/L)	Phosphate (mmol/L)
CN	34.0 ± 2.12[a]	0.37 ± 0.22[ab]	11.53 ± 0.48[a]	7.99 ± 0.91[a]
LD-S-AgNPs	30.33 ± 4.37[a]	0.45 ± 0.05[ab]	13.4 ± 0.75[b]	9.7 ± 0.69[b]
MD-S-AgNPs	33.5 ± 1.32[a]	0.58 ± 0.24[b]	12.78 ± 0.37[b]	8.33 ± 0.37[a]
HD-S-AgNPs	30.0 ± 3.92[a]	0.55 ± 0.01[a]	13.08 ± 0.39[b]	8.23 ± 0.49[a]
LD-S-AgNPs-CSCFX	34.6 ± 2.91[a]	0.33 ± 0.05[ab]	13.23 ± 0.25[b]	8.13 ± 0.23[a]
MD-S-AgNPs-CSCFX	36.5 ± 1.55[a]	0.39 ± 0.06 [ab]	13.20 ± 0.35[b]	8.2 ± 0.32[a]
HD-S-AgNPs-CSCFX	36.25 ± 2.17[a]	0.34 ± 0.05[ab]	12.95 ± 0.21[b]	8.1 ± 0.30[a]

CN: Control negative; LD: Low dose (30 mg/Kg body weight); MD: Median Dose (60 mg/Kg body weight); and HD: High Dose (90 mg/Kg body weight); S-AgNPs: Silica coated silver nanoparticles; S-AgNPs-CFX: Silica coated silver nanoparticles loaded with ciprofloxacin. Superscripts on the right of the means indicate statistical differences ($p < 0.05$) between the groups. Values are means ± standard error. Values are means ± standard errors for $N = 4$. Statistical analysis was by one way ANOVA.

Table 4. Lipid profile and hormone values of rats treated with blank and loaded silica-coated silver nanoparticles with ciprofloxacin.

Test Group	Cholesterol (mg/dL)	Triglyceride (TG) (mg/dL)	High-Density Lipoprotein (HDL) (mg/dL)	Low-Density Lipoprotein (LDL) (mg/dL)	Very low-Density Lipoprotein (VLDL)(mg/dL)	Procalcitonin% (PCT)
CN	78.25 ± 11.65[a]	62.75 ± 18.74[a]	18.13 ± 1.95[a]	27.45 ± 5.29[a]	12.55 ± 3.75[a]	0.38 ± 0.03[b]
LD-S-AgNPs	78.0 ± 2.31[a]	99.33 ± 15.93[b]	17.23 ± 1.04[a]	22.77 ± 4.48[a]	19.87 ± 3.19[b]	0.29 ± 0.01[a]
MD-S-AgNPs	80.23 ± 2.46[a]	102.0 ± 7.67[b]	18.9 ± 0.20[a]	24.70 ± 1.59[a]	20.4 ± 1.53[b]	0.36 ± 0.02[ab]
HD-S-AgNPs	74.75 ± 10.55[a]	99.0 ± 5.82[b]	18.05 ± 1.06[a]	23.18 ± 2.189[a]	19.8 ± 1.16[b]	0.32 ± 0.04[ab]
LD-S-AgNPs-CSCFX	78.5 ± 1.94[a]	88.50 ± 9.95[ab]	20.38 ± 0.96[b]	25.08 ± 0.21[a]	17.65 ± 1.97[ab]	0.38 ± 0.03[b]
MD-S-AgNPs-CSCFX	80.36 ± 9.11[a]	93.75 ± 8.29[ab]	18.55 ± 1.18[a]	23.90 ± 2.25[a]	18.75 ± 1.66[ab]	0.37 ± 0.02 [ab]
HD-S-AgNPs-CSCFX	74.5 ± 4.17[a]	72.0 ± 1.63[ab]	17.4 ± 0.426[a]	22.55 ± 1.07[a]	14.3 ± 0.33[ab]	0.34 ± 0.03[ab]

CN: Control negative; LD: Low dose (30 mg/Kg body weight); MD: Median Dose (60 mg/Kg body weight); and HD: High Dose (90 mg/Kg body weight); S-AgNPs: Silica coated silver nanoparticles; S-AgNPs-CFX: Silica coated silver nanoparticles loaded with ciprofloxacin. Superscripts on the right of the means indicate statistical differences ($p < 0.05$) between the groups. Values are means ± standard error. Values are means ± standard errors for $N = 4$. Statistical analysis was by one way ANOVA.

Table 5A. Hematological values of rats treated with blank and loaded silica-coated silver nanoparticles with ciprofloxacin.

T Test Group	Red Blood Cell (RBC) (10^6/µL)	Hemoglobin (Hgb) (g/dL)	Hematocrit% (HCT)	Mean Corpuscular Volume (MCV) (µmol)	Mean Corpuscular Hemoglobin (MCH) (Pg)	Mean Corpuscular Hemoglobin Concentration (MCHC) (g/dL)	RDWC%	RDWS (µm)
CN	5.93 ± 0.40[a]	13.98 ± 0.84[a]	45.78 ± 3.20[a]	71.55 ± 1.7[a]	21.95 ± 1.13[a]	30.65 ± 0.96[a]	18.18 ± 0.74[a]	49.5 ± 42.88[a]
LD-S-AgNPs	6.02 ± 0.17[a]	14.13 ± 0.31[a]	43.7±.97[a]	72.65 ± 1.34[a]	23.48 ± 45[ab]	32.35 ± 0.94[a]	17.8 ± 0.51[a]	49.4 ± 40.77[a]
MD-S-AgNPs	6.16 ± 0.16[a]	14.4 ± 0.27[a]	44.8 ± 1.69[a]	72.7 ± 1.81[a]	23.4 ± 0.63[ab]	32.23 ± 0.85[a]	16.3 ± 0.69[a]	43.73 ± 35.89[a]
HD-S-AgNPs	6.02 ± 0.21[a]	14.28 ± 0.47[a]	45.2 ± 1.53[a]	75.43 ± 3.98[a]	23.75 ± 0.15[ab]	31.73 ± 1.58[a]	17.88 ± 1.47[a]	52.6 ± 21.52[a]
LD-S-AgNPs-CSCFX	6.39 ± 0.199[a]	15.1 ± 0.17[a]	47.73 ± 1.28[a]	75.08 ± 3.97[a]	23.7 ± 0.70[ab]	31.73 ± 0.71[a]	17.35 ± 1.55[a]	48.65 ± 27.61[a]
MD-S-AgNPs-CSCFX	5.97 ± 0.166[a]	14.63 ± 0.13[a]	44.85 ± 0.66[a]	75.18 ± 1.29[a]	24.55 ± 0.86[b]	32.65 ± 0.66[a]	15.9 ± 0.22[a]	44.05 ± 41.93[a]
HD-S-AgNPs-CSCFX	6.14 ± 0.34[a]	14.4 ± 0.46[a]	44.33 ± 1.28[a]	72.68 ± 2.93[a]	23.55 ± 0.59[ab]	32.48 ± 0.69[a]	17.73 ± 1.18[a]	49.85 ± 32.35[a]

Table 5B. Hematological values of rats treated with blank and loaded silica-coated silver nanoparticles with ciprofloxacin.

Test Group	Platelets (PLT) (103/µL)	Mean Platelet Volume (MPV) (µm3)	Platelet Distribution Width% (PDW)	Platelet-Large Cell Ratio% (PLCR)	White Blood Cells (WBC) (103 /µL)	Lymphocyte%	Monocyte%	Granulocyte%
CN	456.0 ± 59.17[b]	8.58 ± 0.73[b]	17.7 ± 0.73[a]	17.35 ± 5.35[ab]	7.8±.69[a]	74.90 ± 4.84[a]	6.98 ± 0.73[b]	18.1 ± 4.74[b]
LD-S-AgNPs	303.75 ± 16.40[a]	9.65 ± 0.29[a]	16.7 ± 0.88[a]	17.3 ± 2.15 [cd]	10.23±.84[a]	83.45 ± 1.67[b]	5.43 ± 0.67[ab]	11.13 ± 1.01[a]
MD-S-AgNPs	443.25 ± 26.73[b]	8.25 ± 0.20[ab]	17.25 ± 1.04[a]	14.6 ± 1.81[a]	14.58 ± 2.14[b]	87.73±.54[b]	4.98 ± 0.23[a]	7.3 ± 0.53[a]
HD-S-AgNPs	406.75 ± 57.79[ab]	7.88 ± 0.31[ab]	17.05 ± 0.75[a]	12.5 ± 1.87[a]	15.23 ± 1.37[b]	86.88 ± 2.48[b]	4.98±.71[a]	8.15 ± 1.80[a]
LD-S-AgNPs-CSCFX	373.5 ± 33.93[ab]	10.25 ± 0.45[b]	17.25 ± 0.76[a]	19.45 ± 3.73[d]	15.95±.96[b]	83.18 ± 2.72[b]	5.15 ± 0.46[ab]	10.68 ± 2.23[a]
MD-S-AgNPs-CSCFX	419.5 ± 15.44[ab]	8.85 ± 0.12[ab]	18.3 ± 0.39[a]	18.35 ± 1.1[abc]	15.55 ± 1.95[b]	87.23±.74[b]	5.3 ± 0.51[ab]	7.48 ± 0.51[a]
HD-S-AgNPs-CSCFX	359.5 ± 21.75[ab]	9.53 ± 0.23[ab]	17.50 ± 1.12[a]	24.95 ± 3.07[bcd]	18.73 ± 1.63[b]	89.38±.87[b]	5.05 ± 0.44[a]	5.58 ± 0.50[a]

grade vacuolar degeneration within the renal tubular epithelium and very mild vascular congestion (Figure 7). Control negative group received (D.W), showed no visible morphological deviation, apparent by representative glomeruli and regular Bowman's capsule (BC). Renal tubules (RT) as well exhibit no significant lesions except for slight and non-significant tubular dilation. Low dose group treated with 30 mg/kg of S-AgNPs-CSCFX, showed non-significant to moderate cellular swelling within the renal tubular epithelia. The section also reveals many areas of typically arranged renal tubules (RT) together with renal glomeruli (GL) with no clear morphological changes. Medium dose group, treated 60 mg/kg of S-AgNPs-CSCFX, showed moderate cellular swelling within the renal tubular epithelium (CS). The section also demonstrates some area of vascular congestion (VC) together
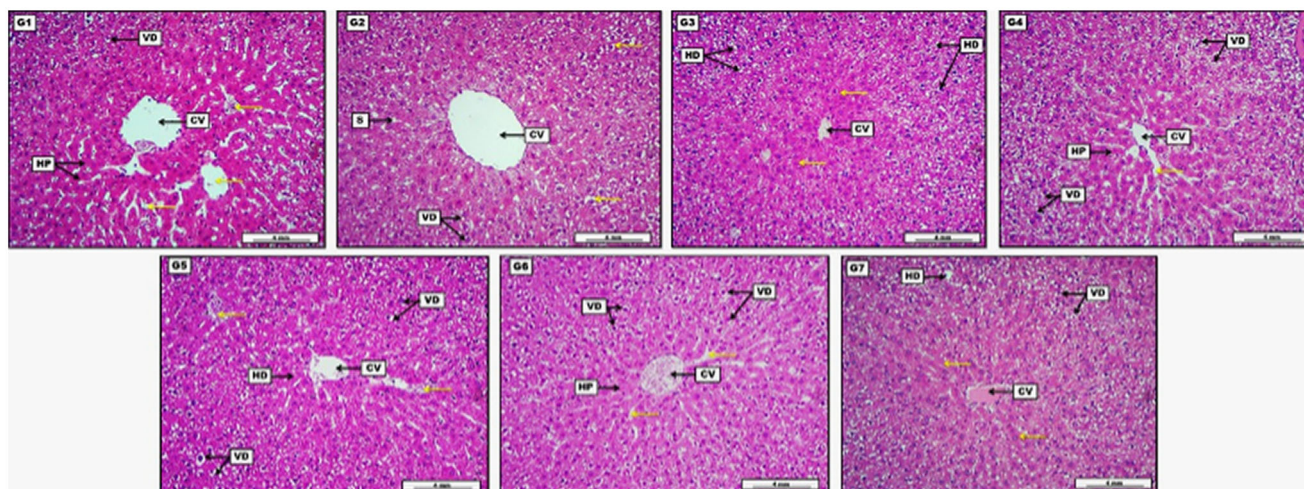
Figure 6. Photomicrograph of liver from groups; G1: Control negative group received (D.W); G2: Low dose group (G2) treated with 30 mg/kg of S-AgNPs-CSCFX; G3: Medium dose group (G3), treated with 60 mg/kg of S-AgNPs-CSCFX; G4: High dose group (G4) treated with 90 mg/kg of S-AgNPs-CSCFX; G5: Low dose group (G5) treated with 30 mg/kg of blank S-AgNPs; G6: Medium dose group (G6) treated with 60 mg/kg of blank S-AgNPs; G7: High dose group (G7) treated with 90 mg/kg of blank S-AgNPs. H&E. Scale bar: 4 mm.
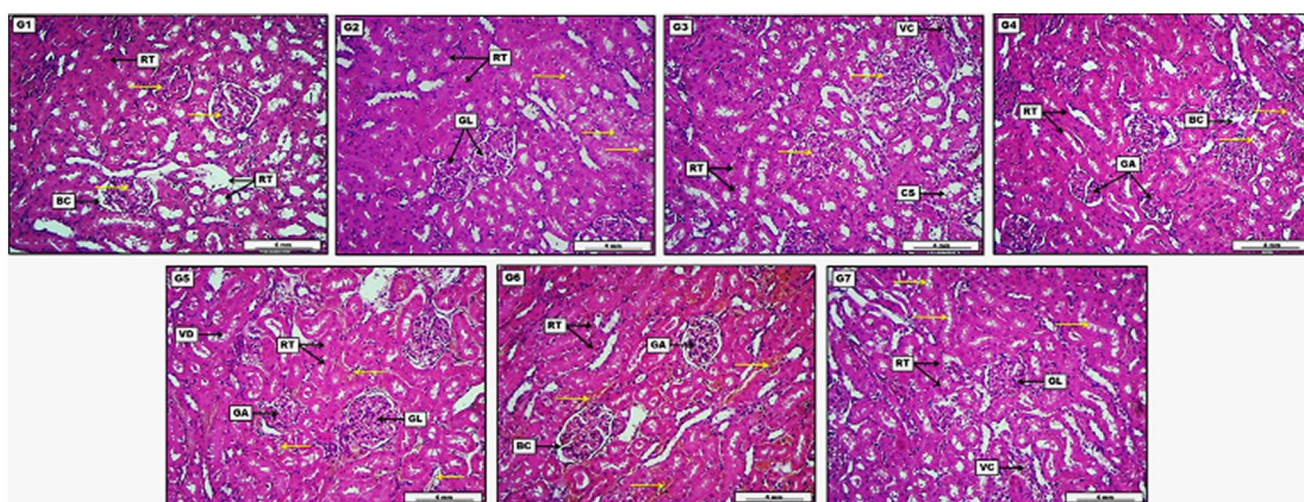

Figure 7. Photomicrograph of kidney from groups; G1: Control negative group received (D.W); G2: Low dose group (G2) treated with 30 mg/kg of S-AgNPs-CSCFX; G3: Medium dose group (G3), treated 60 mg/kg of S-AgNPs-CSCFX; G4: High dose group (G4) treated with 90 mg/kg of S-AgNPs-CSCFX; G5: Low dose group (G5), treated with 30 mg/kg of blank S-AgNPs; G6: Medium dose group (G6), treated with 60 mg/kg of blank S-AgNPs; G7: high dose group (G7), treated with 90 mg/kg of blank S-AgNPs; H&E. Scale bar: 4 mm.

with normally appeared renal glomeruli. High dose group treated with 90 mg/kg of S-AgNPs-CSCFX, presented severe and significant glomerular atrophy (GA), evident by obvious widening of the Bowman's capsule (BC). In addition, the section shows area of cellular swelling within the renal tubular epithelia, together with usually appeared renal tubules (RT). Low dose group, treated with 30 mg/kg of blank S-AgNPs, demonstrated mild to moderate glomerular atrophy (GA) as well as vascular congestion. Renal tubular epithelium (RT) reveals area of vacuolar degeneration (VD). Moreover, many areas show typically arranged tubules. Medium dose group treated with 60 mg/kg of blank S-AgNPs, showed significant vascular congestion within the renal blood vessels. In addition, a moderate glomerular atrophy (GA) manifested by sensible spreading of Bowman's space (BC) was observed. Renal tubular epithelium (RT) expresses slight hydropic degeneration. High dose group treated with 90 mg/kg of blank S-AgNPs, displayed significant cellular swelling within the renal tubular epithelium. The section also demonstrates moderate vascular congestion (VC), together with areas of ordinary appeared renal glomerular structure (GL) and tubules (RT).

4. Discussion

S-AgNPs-CSCFX microparticles were prepared successfully using three fluid nozzle spray drying. Successful encapsulation was achieved and confirmed using surface techniques (EDX and XRPD) as well as using bulk/morphology using SEM and TEM. When chitosan was present the particles seemed to aggregate which may suggest that the polymer/CFX mixture partially segregated into a different phase from the core liquid (silica coated Ag). While this is a desired outcome in which two phases were obtained, it also suggests that further optimisation was needed to ensure formation of core/shell structures. Molecular interactions showed clear shift in FTIR peaks of CFX when chitosan was present confirming the presence of solid dispersion coating the core silica coated silver nanoparticles. Presence of Ag, as shown in EDX and XRPD

data, indicate incomplete coating by silica which have resulted in detecting traces of Ag. However, considering the dilution effect (i.e. intensity of peaks is lower due to lower Ag ratio), the results confirmed the formation of a chitosan/CFX coat around the silver coated silica nanoparticles. Zeta potential measurements showed consistency with other data showing significant enhancement in zeta potential of chitosan containing microparticles to 25.2 ± 5.52 mv. It is clear from these results that the surface has changed according to the composition with a noticeable difference when chitosan was incorporated reflected by the positive zeta value. When compared with reported values, the positive charge obtained in the prepared particles reflects success of three fluid nozzle spray drying to prepare cationic microparticles. It is interesting to observe that the silica nanoparticles formed spherical micro aggregates which were ultimately coated by the chitosan/CFX coat. This added to the control in dissolution which was seen in the TEM images indicating release of the entrapped silver.

Investigation of the oral intake of blank and loaded AgNPs was carried out on body weight, biochemical/hematological parameters, and histopathological observations using oral doses for 21 days. Body weight is widely utilized as a reliable indicator of the substance toxicity (Nirogi et al. 2014). According to several studies, contact to gold (Xia et al. 2014), nickel (Kong et al. 2014), and silver (Wen et al. 2017) NPs can cause loss of body weight. Despite this, there is contradictory evidence in the literature (Gromadzka-Ostrowska et al. 2012; Yin et al. 2015). During the treatment period, we assessed the rats' body weight and discovered that the rats' weight increased dramatically with age after all treatments. These results agreed with Adeyemi and Adewumi (2014) who found that the body weights of the rats treated with AgNPs increased at all dosages, and the weight gains were significant in the 1000 mg/kg for 2 weeks and 5000 mg/kg for 3 weeks (Adeyemi and Adewumi 2014). However, findings contradict Zhang et al. (2013) who found that the male rat body weight was sensitive to AgNPs, and the intravenous (iv) dosage of NPs (20 and 40 mg/kg) caused body weight loss (Zhang et al. 2013). Whereas Kim et al. (2008) demonstrated that the male/female Sprague Dawley rats did not display any substantial body weight changes concerning the various doses of AgNPs (30–1000 mg/kg) during the 4 weeks experiment (Kim et al. 2008). Similarly, Sung et al. (2011) found that AgNPs inhalation (0.94×10^6 to 3.08×10^6 particle/cm^3) did not reduce male and female Sprague Dawley's body weight during the 2-week observation period (Sung et al. 2011). It was reported that fluctuation in the body weight in animals treated with AgNPs might be related to the method of NPs preparation, NPs content, duration of administration, administration route, and dose (Moradi-Sardareh et al. 2018).

Assessment of liver and kidney function is of major significance in measuring the toxic characteristics of extracts, chemicals, and drugs. They are major target organs for several substances due to their critical role in various body processes, including detoxification and excretion (Al-Doaiss et al. 2020). In this study, there were no substantial changes in the mean value of all biochemical parameters (except for AST) in all treated groups compared to the healthy controls. The renal and hepatic enzyme level alterations may be an adaptive strategy used by the animals to counteract the stress brought on by AgNP exposure (Adeyemi and Adewumi 2014). In the past several years, because of the importance of these enzymes, studies of serum aminotransferases have evolved into a widely used indicator of hepatotoxicity (Al-Doaiss et al. 2020). These enzymes are often found in the liver and other

tissues, where they participate in the transamination of amino acids, a process that helps the body use energy.

The AST and ALT, however, may escape into the blood stream in situations of cellular injury, resulting in increased activity (Bello et al. 2016). Our results agreed with the findings of Alwan et al. (2021) who found that AgNPs (0.85, 1.76, and 3.53 mg/kg) did not induce any fluctuations in the mean of biochemical parameters (AST, ALT, urea, and creatinine) (Alwan et al. 2021). Whereas Adeyemi and Adewumi (2014) displayed that AgNPs significantly decreased levels of serum and tissue AST, ALT, and ALP at 100 mg/kg (Adeyemi and Adewumi 2014). In contrast, treatment of adult male Balb/C mice with 35 intraperitoneal (ip) injections of AgNPs (1.0 mg/kg) using particle sizes of 10, 20, 40, 60, and 100 nm; markedly elevated hepatic and renal biomarkers (Al-Doaiss et al. 2020). Abbas et al. (2011) indicated that AgNPs markedly inhibited AST and ALT in rats due to Ag interaction with functional groups (thiol) of these enzymes, resulting in protein denaturation and inactivation (Abbas et al. 2011). Moreover, treating rats with blank and loaded AgNPs did not elevate lipid profile tests (except TG and VLDL) and prolactin values. In this respect, Kim et al. (2008) found substantial elevation in TC in both the high-dose (1000 mg/kg AgNPs) ($p < 0.05$) male rats and the middle and high-dose (300 and 1000 mg/kg AgNPs, respectively) ($p < 0.01$) female rats with no changes to TG values (Kim et al. 2008), while Sulaiman et al. (2015) found depletion in the level of HDL by AgNPs exposure (10, 50, and 100 mg/kg) (Sulaiman et al. 2015). On the other hand, Ali and Khudair (2019) found that AgNPs loaded *Nigella sativa* (25–50 mg/kg) receded a case of dyslipidemia in treated adult male rats (Ali and Khudair 2019), while Dandapat et al. (2021) declared that AgNPs loaded *Ganoderma applanatum* (400 mg/kg) increased hyperthyroid and hypolipidemic activity (Dandapat et al. 2021). Moreover, Elle et al. (2013) reported that AgNPs (500 mg/kg) resulted in cholesterolemia (9.5%), increased LDL (30%), but lowered TG (41%) (Elle et al. 2013). Regarding the hematological parameters, AgNPs significantly reduced WBC, lymphocyte, monocyte, and granulocyte values since others blood tests were not changed considerably in treated animals with various doses of blank and loaded AgNPs compared to the healthy controls. In this regard, Park (2013) found decreased RBC counts, HCT, and Hgb in the Ag-treated groups, while raised PLT levels and MPV were found in the AgNP-treated rats. In contrast, MCV, MCH, MCHC, RDW, hemoglobin distribution width (HDW), WBC count, and percent differential leukocytes were not changed (Park 2013). In contrast to our results, MCV in high-dose male (1000 mg/kg AgNPs), RBC, Hgb, and HCT in both the middle and high-dose (300 and 1000 mg/kg AgNPs, respectively) female rats were increased significantly in a research conducted by Kim et al. (2008). Moreover, Heydrnejad et al. (2015) showed that RBC, Hb, and HCT did not vary significantly in the AgNPs (20 and 50 ppm) treated male/female mice (Heydrnejad et al. 2015), as well as Qin et al. 2017, concluded that RBC increased and PLT decreased significantly in male rats treated with 1.0 mg/kg AgNPs ($p < 0.05$) (Qin et al. 2017). Furthermore, reports indicate that AgNPs affect hematological indices in birds. Loghman et al. (2012) found that broiler chickens receiving AgNPs had lower WBC, RBC, and Hgb values (Loghman et al. 2012). The histopathological findings of the vital organs of rats treated with various doses (30, 60, and 90 mg/kg) of the blank and loaded AgNPs showed no remarkable alterations in the liver and kidneys compared to controls. This was in line with the work of (Alwan et al. 2021) who mentioned that AgNPs did not induce any changes in histopathologic features of the liver and kidneys (Alwan et al. 2021). Controversially, these findings differed from

the work of Sardari et al. (2012) who highlighted how repeated oral administration of AgNPs caused hepatotoxicity and discovered that the process of phagocytosis, which removes NPs from the liver by macrophages, increased the levels of oxygen radicals in the blood (Sardari et al. 2012). Moreover, Wen et al. (2017) found serious cell degeneration and necrosis in the liver/kidneys rat treated with AgNP reliable with the bio-distribution and biochemical outcomes and due to the high Ag amounts that collected in these organs (Wen et al. 2017). Additionally, Adeyemi et al. (2015) showed diverse inimical histopathological alterations to renal cellular architecture in rats orally administered with AgNPs (1000–5000 mg/kg) (Adeyemi et al. 2015). Loghman et al. (2012) determined that the cytotoxicity of AgNPs to mitochondrial action raised with the rise in AgNPs amount, causing a radical decreasing in mitochondrial action, enhanced membrane leakage, necrosis, and initiation of apoptosis in chicken liver cells (Loghman et al. 2012).

5. Conclusions

The results showed the feasibility of using three fluid nozzle spray drying to form silver coated silica nanoparticles encapsulated within ciprofloxacin and chitosan matrix. S-AgNPs and S-AgNPs-ciprofloxacin nanoparticles oral usage had no adverse effects, and they appear to be safe if they are used in human for treating infectious diseases. This requires further studies to confirm toxic dose levels in humans which will be the focus of future studies. These findings demonstrate the effectiveness of these particles and the potential use in targeting different systemic and regional bacterial infections.

Author contsributions

The study was planned, designed and supervised by HSR and SAA. The data acquisition was done by DDM. The data analysis was done by SAA. The nanoparticle preparation and characterisation was done by TZB and HAO. The manuscript drafted and revised by HRS, SAA and HAO.

Institutional review board Statement

The study protocol was approved by the Ethic Committee of the College of Pharmacy, University of Sulaimani, Kurdistan/Iraq. All experiments were carried out following the Organization Economic Cooperation and Development (OECD) guideline (National Research Council 2011) and following the animal ethics guidelines of the College of Pharmacy, the University of Sulaimani, Sulaimaniyah, Iraq, to minimize the suffering of animals (No. PH49-22 on April 18, 2022).

Disclosure statement

No potential conflict of interest was reported by the author(s).

ORCID

Hisham Al-Obaidi (ID) http://orcid.org/0000-0001-9735-0303

Data availability Statement

The datasets used and/or analyzed during the current study are available from the corresponding author on reasonable request.

References

Abbas SAR, Abdullah AH, Sada S, Ali A. 2011. The effects of gold and silver nanoparticles on transaminase enzymes activities. Inter J Chem Res. 1(4):1–11.

Adeyemi OS, Adewumi I. 2014. Biochemical evaluation of silver nanoparticles in wistar rats. Inter Scholarly Res Notices. 2014:1–8.

Adeyemi OS, Adewumi I, Faniyan TO. 2015. Silver nanoparticles influenced rat serum metabolites and tissue morphology. J Basic Clin Physiol Pharmacol. 26(4):355–361.

Al-Doaiss AA, Jarrar Q, Alshehri M, Jarrar B. 2020. In vivo study of silver nanomaterials' toxicity with respect to size. Toxicol Ind Health. 36(8):540–557.

Al-Obaidi H, Kalgudi R, Zariwala MG. 2018. Fabrication of inhaled hybrid silver/ciprofloxacin nanoparticles with synergetic effect against Pseudomonas aeruginosa. Eur J Pharm Biopharm. 128: 27–35.

Alavi M, Rai M. 2019. Recent progress in nanoformulations of silver nanoparticles with cellulose, chitosan, and alginic acid biopolymers for antibacterial applications. Appl Microbiol Biotechnol. 103(21-22):8669–8676.

Ali ZS, Khudair KK. 2019. Synthesis, Characterization of Silver Nanoparticles Using Nigella sativa Seeds and Study Their Effects on the Serum Lipid Profile and DNA Damage on the Rats' Blood Treated with Hydrogen Peroxide: zainab Sattar Ali and Khalisa Khadim Khudair. Iraqi J Vet Med. 43(2):23–37.

Alwan S, Al-Saeed M, Abid H. 2021. Safety assessment and biochemical evaluation of biogenic silver nanoparticles (using bark extract of C. zeylanicum) in Rattus norvegicus rats: safety of biofabricated AgNPs (using Cinnamomum zeylanicum extract). Baghdad J Biochem Appl Biol Sci. 2(03):133–145.

Bello I, Bakkouri AS, Tabana YM, Al-Hindi B, Al-Mansoub MA, Mahmud R, Asmawi MZ. 2016. Acute and sub-acute toxicity evaluation of the methanolic extract of Alstonia scholaris stem bark. Medical Sciences. 4(1):4.

Chen Q, Shah KN, Zhang F, Salazar AJ, Shah PN, Li R, Sacchettini JC, Wooley KL, Cannon CL. 2019. Minocycline and silver dual-loaded polyphosphoester-based nanoparticles for treatment of resistant Pseudomonas aeruginosa. Mol Pharm. 16(4):1606–1619.

Crissman JW, Goodman DG, Hildebrandt PK, Maronpot RR, Prater DA, Riley JH, Seaman WJ, Thake DC. 2004. Best practices guideline: toxicologic histopathology. Toxicol Pathol. 32(1):126–131.

Dandapat S, Srivastava R, Sinha MP, 2021. Study on impact of silver nanoparticles synthesized using aqueous extract of Ganoderma applanatum on thyroid and lipid parameters of albino rat: impact of silver nanoparticles on thyroid and lipid profile. Anales de Biología. 43:123–137.

Elle RE, Gaillet S, Vidé J, Romain C, Lauret C, Rugani N, Cristol J, Rouanet J. 2013. Dietary exposure to silver nanoparticles in Sprague–Dawley rats: effects on oxidative stress and inflammation. Food Chem Toxicol. 60:297–301.

Farooq U, Ahmad T, Khan A, Sarwar R, Shafiq J, Raza Y, Ahmed A, Ullah S, Rehman NU, Al-Harrasi A. 2019. Rifampicin conjugated silver nanoparticles: a new arena for development of antibiofilm potential against methicillin resistant Staphylococcus aureus and Klebsiella pneumoniae. Int J Nanomedicine. 14:3983–3993.

Feng C, Li J, Kong M, Liu Y, Cheng XJ, Li Y, Park HJ, Chen XG. 2015. Surface charge effect on mucoadhesion of chitosan based nanogels for local anti-colorectal cancer drug delivery. Colloids Surf B Biointerfaces. 128:439–447.

Gromadzka-Ostrowska J, Dziendzikowska K, Lankoff A, Dobrzyńska M, Instanes C, Brunborg G, Gajowik A, Radzikowska J, Wojewódzka M, Kruszewski M. 2012. Silver nanoparticles effects on epididymal sperm in rats. Toxicol Lett. 214(3):251–258.

Guadarrama-Escobar OR, Serrano-Castaneda P, Anguiano-Almazan E, Vazquez-Duran A, Pena-Juarez MC, Vera-Graziano R, Morales-Florido MI, Rodriguez-Perez B, Rodriguez-Cruz IM, Miranda-Calderon JE, et al. 2023. Chitosan nanoparticles as oral drug carriers. Int J Mol Sci. 24(5):4289.

Heydrnejad MS, Samani RJ, Aghaeivanda S. 2015. Toxic effects of silver nanoparticles on liver and some hematological parameters in male and female mice (Mus musculus). Biol Trace Elem Res. 165(2):153–158.

Jarvie HP, Al-Obaidi H, King SM, Bowes MJ, Lawrence MJ, Drake AF, Green MA, Dobson PJ. 2009. Fate of silica nanoparticles in simulated primary wastewater treatment [Research Support, Non-U.S. Environ Sci Technol. 43(22):8622–8628. eng.

Kaur A, Preet S, Kumar V, Kumar R, Kumar R. 2019. Synergetic effect of vancomycin loaded silver nanoparticles for enhanced antibacterial activity. Colloids Surf B Biointerfaces. 176:62–69.

Kim YS, Kim JS, Cho HS, Rha DS, Kim JM, Park JD, Choi BS, Lim R, Chang HK, Chung YH, et al. 2008. Twenty-eight-day oral toxicity, genotoxicity, and gender-related tissue distribution of silver nanoparticles in Sprague-Dawley rats. Inhal Toxicol. 20(6):575–583.

Kobayashi Y, Katakami H, Mine E, Nagao D, Konno M, Liz-Marzan LM. 2005. Silica coating of silver nanoparticles using a modified stober method. J Colloid Interface Sci. 283(2):392–396.

Kong L, Tang M, Zhang T, Wang D, Hu K, Lu W, Wei C, Liang G, Pu Y. 2014. Nickel nanoparticles exposure and reproductive toxicity in healthy adult rats. Int J Mol Sci. 15(11):21253–21269.

Kumar SSD, Rajendran NK, Houreld NN, Abrahamse H. 2018. Recent advances on silver nanoparticle and biopolymer-based biomaterials for wound healing applications. Int J Biol Macromol. 115:165–175.

Lee SH, Jun B-H. 2019. Silver nanoparticles: synthesis and application for nanomedicine. IJMS. 20(4):865.

Liu Q, Zhang Y, Huang J, Xu Z, Li X, Yang J, Huang H, Tang S, Chai Y, Lin J, et al. 2022. Mesoporous silica-coated silver nanoparticles as ciprofloxacin/siRNA carriers for accelerated infected wound healing. J Nanobiotechnol. 20(1):1–16.

Loghman A, Iraj SH, Naghi DA, Pejman M. 2012. Histopathologic and apoptotic effect of nanosilver in liver of broiler chickens. Afr J Biotechnol. 11(22):6207–6211.

Marin S, Mihail Vlasceanu G, Elena Tiplea R, Raluca Bucur I, Lemnaru M, Minodora Marin M, Mihai Grumezescu A. 2015. Applications and toxicity of silver nanoparticles: a recent review. Curr Top Med Chem. 15(16):1596–1604.

Mohammed A, Zurek J, Madueke S, Al-Kassimy H, Yaqoob M, Houacine C, Ferraz A, Kalgudi R, Zariwala MG, Hawkins N, et al. 2020. Generation of high dose inhalable effervescent dispersions against pseudomonas aeruginosa biofilms. Pharm Res. 37(8):150.

Moradi-Sardareh H, Basir HRG, Hassan ZM, Davoudi M, Amidi F, Paknejad M. 2018. Toxicity of silver nanoparticles on different tissues of Balb/C mice. Life Sci. 211:81–90.

National Research Council 2011. Guide for the care and use of laboratory animals. 8th ed. Wash, DC: National Academy Press.

Nirogi R, Goyal VK, Jana S, Pandey SK, Gothi A. 2014. What suits best for organ weight analysis: review of relationship between organ weight and body/brain weight for rodent toxicity studies. Int J Pharm Sci Res. 5(4):1525–1532.

Park K. 2013. Toxicokinetic differences and toxicities of silver nanoparticles and silver ions in rats after single oral administration. J Toxicol Environ Health A. 76(22):1246–1260.

Pedreiro LN, Boni FI, Cury BSF, Ferreira NN, Gremiao MPD. 2022. Solid dispersions based on chitosan/hypromellose phthalate blends to modulate pharmaceutical properties of zidovudine. Pharm Dev Technol. 27(5):615–624.

Qin G, Tang S, Li S, Lu H, Wang Y, Zhao P, Li B, Zhang J, Peng L. 2017. Toxicological evaluation of silver nanoparticles and silver nitrate in rats following 28 days of repeated oral exposure. Environ Toxicol. 32(2):609–618.

Sardari RRR, Zarchi SR, Talebi A, Nasri S, Imani S, Khoradmehr A, Sheshde SAR. 2012. Toxicological effects of silver nanoparticles in rats. Afric J Microbiol Res. 6(27):5587–5593.

Sulaiman FA, Adeyemi OS, Akanji MA, Oloyede HOB, Sulaiman AA, Olatunde A, Hoseni AA, Olowolafe YV, Nlebedim RN, Muritala H, et al. 2015. Biochemical and morphological alterations caused by silver nanoparticles in Wistar rats. J Acute Med. 5(4):96–102.

Sung JH, Ji JH, Song KS, Lee JH, Choi KH, Lee SH, Yu IJ. 2011. Acute inhalation toxicity of silver nanoparticles. Toxicol Ind Health. 27(2):149–154.

Ways TM, Lau W, Khutoryanskiy V. 2018. Chitosan and its derivatives for application in mucoadhesive drug delivery systems. Polymers. 10(3):267.

Wen H, Dan M, Yang Y, Lyu J, Shao A, Cheng X, Chen L, Xu L. 2017. Acute toxicity and genotoxicity of silver nanoparticle in rats. PLoS One. 12(9):e0185554.

Xia D-L, Wang Y-F, Bao N, He H, Li X-d, Chen Y-P, Gu H-Y. 2014. Influence of reducing agents on biosafety and biocompatibility of gold nanoparticles. Appl Biochem Biotechnol. 174(7):2458–2470.

Yin N, Yao X, Zhou Q, Faiola F, Jiang G. 2015. Vitamin E attenuates silver nanoparticle-induced effects on body weight and neurotoxicity in rats. Biochem Biophys Res Commun. 458(2):405–410.

Zhang Y, Ferguson SA, Watanabe F, Jones Y, Xu Y, Biris AS, Hussain S, Ali SF. 2013. Silver nanoparticles decrease body weight and locomotor activity in adult male rats. Small. 9(9-10):1715–1720.